Glaucoma

Heterozygous *Pitx2* Null Mice Accurately Recapitulate the Ocular Features of Axenfeld-Rieger Syndrome and Congenital Glaucoma

Lisheng Chen[1] and Philip J. Gage[1,2]

[1]Department of Ophthalmology & Visual Sciences, University of Michigan, Ann Arbor, Michigan, United States
[2]Department of Cell & Developmental Biology, University of Michigan, Ann Arbor, Michigan, United States

PURPOSE. The purpose of this analysis was to assess the utility of $Pitx2^{+/-}$ mice as a model for the ocular features of Axenfeld-Rieger Syndrome and for congenital glaucoma.

METHODS. Eyes of $Pitx2^{+/-}$ and wild-type littermates were examined clinically using optical coherence tomography (OCT) and fundus photography. Intraocular pressures were measured using a TonoLab rebound tonometer. Eyes were examined histologically to assess PITX2 expression, structural integrity, and optic nerve and ganglion cell content.

RESULTS. PITX2 is present postnatally in the corneal endothelium and stroma, iris stroma, trabecular meshwork, and Schlemm's canal. Reduced central corneal thickness, iris defects, and iridicorneal adhesions are all prevalent in $Pitx2^{+/-}$ eyes. Although optic nerve heads appear normal at postnatal day 7, IOP is elevated and optic nerve head cupping is fully penetrant in $Pitx2^{+/-}$ eyes by 3 weeks of age. Neurodegeneration is present in a significant percentage of optic nerves from $Pitx2^{+/-}$ mice by 3 weeks of age, and is fully penetrant by 2 months of age. $Pitx2^{+/-}$ eyes show significant reductions in specifically ganglion cell density in all four quadrants by 2 months of age.

CONCLUSIONS. $Pitx2^{+/-}$ mice model the major ocular features of Axenfeld-Rieger Syndrome and will be an important resource for understanding the molecular mechanisms leading to anterior segment dysgenesis and a high prevalence of glaucoma in this disease. In addition, these mice may provide an efficient new model for assessing the molecular events in glaucoma more generally, and for developing and testing new treatment paradigms for this disease.

Keywords: *Pitx2*, homeodomain, mouse model

Glaucoma is an optic neuropathy characterized by optic nerve head damage, loss of retinal ganglion cells (RGCs), and consequently visual field loss. It is the second leading cause of irreversible blindness and expected to affect 111.8 million people worldwide by the year of 2040.[1] Glaucoma is generally characterized into two major subtypes based on the status of the internal drainage system: open angle glaucoma and angle closure glaucoma.[2,3] The pathology of glaucoma remains largely unclear, although it is known that multiple risk factors play roles. Among these, IOP is a strong and the only therapeutically modifiable risk factor.[4,5] Normally, the IOP is a balance of aqueous humor production by the ciliary body and aqueous humor drainage through the internal outflow system.[2,3,6] Elevated pressure increases the stress and strain within and across the laminar region of optic nerve head, the primary site of injury in glaucoma, resulting in a translaminar pressure gradient and consequently downstream molecular and cellular events involved in pathology of glaucoma disease.[6–8]

Glaucoma is a complex and highly heterogeneous group of ocular diseases that results from both genetic and environmental factors, which makes elucidating the underlying biological pathways difficult. Genetic studies in mice have proven to be an important means to investigate genes and pathologic mechanisms that cause glaucoma in a physiological context.

The unique ability to edit the mouse genome and analyze naturally occurring or engineered mutations on different defined, inbred genetic backgrounds, thereby permitting the distinction between genetic background versus environmental effects, makes mouse models an informative tool for understanding human disease.[9,10] For example, genetic analysis of DBA/2J mice allowed the identification of two genes (*Gpnmb* and *Tyrp1*) that when mutated cause a progressive form of pigmentary glaucoma,[11,12] and transgenic mice expressing either disease-causing mutations in human or mouse Myocilin exhibit pathologic and clinical changes that are comparable to those observed in human patients with open angle glaucoma.[13,14] However, there are likely numerous molecular pathways that control susceptibility to the disease and no single mouse model has been described that is sufficient to study all aspects of glaucoma.[15] In addition, the age of disease onset for currently described genetic mouse models is very late (typically ≥ 8 months), which is a practical impediment to progress as it slows experimentation and raises costs. For these reasons, the identification of new genetic mouse models, particularly those developing earlier onset of symptoms would be very advantageous.

Heterozygous mutations in the human paired-like homeodomain transcription factor gene *PITX2* are a significant cause

of Axenfeld-Rieger Syndrome (ARS), an autosomal dominant disorder that affects multiple organ systems. In the eye, this condition manifests with a varying degree of anterior segment dysgenesis, including posterior embryotoxon, iris hypoplasia, corectopia, polycoria, and peripheral anterior synechiae (iridocorneal adhesions).[16-18] The anomalies in anterior segment frequently result in elevated IOP, which is thought to underlie the more than 50% risk of congenital or very early-onset glaucoma in these patients.[16,17,19,20] An animal model that accurately recapitulates postnatal ocular features of ARS would be an important resource in the future for understanding the effects of reduced *PITX2* on the eye morphogenesis during development, identifying disrupted genetic pathways in the affected structure(s), and potentially developing new therapies for ARS, and poorly understood disease. We previously used global and conditional *Pitx2* knockout mice to show that anterior segment development is arrested at early stages of eye development, prior to the emergence of structures involved in IOP homeostasis and development of the optic nerve, meaning that these animals are not useful as models for studying the development of glaucoma in ARS.[21,22] Therefore, a useful model to study the molecular mechanisms leading to ARS remains to be identified.

In this study, we examined postnatal heterozygous *Pitx2* mice (*Pitx2*^{+/−}) clinically and histologically to determine whether ocular features of ARS and glaucoma are present. We show that *Pitx2*^{+/−} mice phenocopy the major anterior segment defects present in ARS patients, and IOP is frequently elevated. Further, optic nerve head cupping and partial to complete degeneration of the optic nerve consistent with glaucoma is present in all *Pitx2*^{+/−} eyes examined by 2 months of age. Retinal ganglion cell density is also reduced in *Pitx2*^{+/−} eyes. Collectively, we conclude that *Pitx2*^{+/−} mice are a useful new model for determining the molecular mechanisms leading to the ocular defects in ARS and events leading to the associated glaucoma.

MATERIALS AND METHODS

Mouse Strains and Animal Husbandry

All experiments were conducted in accordance with the National Institutes of Health Guidelines for the Care and Use of Experimental Animals, and all procedures involving mice were preapproved by the Committee on Use and Care of Animals at the University of Michigan (Ann Arbor, MI, USA) and all animals were treated in accordance with the ARVO Statement for the Use of Animals in Ophthalmic and Vision Research. The relevant cross was *Pitx2*^{+/−} x *C57BL/6J*. The resulting embryos were genotyped as appropriate using PCR-based methods.[21]

Measurement of Intraocular Pressure

Pitx2^{+/−} mice and control littermates were generated for 3-week, 2-, and 4-month old, respectively. Animals were anesthetized by injection of ketamine (100 μg/g) and xylazine (10 μg/g) solution. Intraocular pressure was measured using an iCare Tonolab tonometer (Raleigh, NC, USA), according to the user's manual, in a blinded way. Each measurement was repeated for five times within 6 minutes after administration of anesthesia and the average was used as a final read. All animals were placed in a quiet room approximately 2 hours ahead of measuring for accommodation. All measurements were performed between 2 PM and 4 PM to avoid potential pressure fluctuations.

Spectral-Domain Optical Coherence Tomography

Optical coherence tomography was performed with a SD-OCT system (Bioptigen, Inc., Durham, NC, USA). For anterior segments and angle imaging, a 12-mm telecentric OCT lens was used with reference arm set to 807. A rectangle volume analysis was performed using 33 consecutive B scan lines, each one composed of 1000 A-scans and three frames. The volume size was 1.4×1.4 mm. For optic nerve head imaging, a general mouse OCT lens was used with reference arm set to 1020. A radial volume analysis centered on the optic nerve head was performed, using 33 consecutive B scan lines, each one composed of 1000 A-scans and three frames. The volume diameter was 1.4 mm.

Fundus Photography

General fundus was performed with a commercial camera and imaging system (Micron III; Phoenix Research Labs, Pleasanton, CA, USA), according to the user's manual.

Paraffin Sections, Histochemistry, and Immunostaining

Eyes were enucleated from postnatal pups (10-days, 2-weeks, or 2-months old), fixed in 4% paraformaldehyde diluted in PBS, washed in PBS, dehydrated through graded alcohols, and processed into Paraplast Plus (McCormick Scientific, St. Louis, MO, USA) for paraffin sectioning. Mounted paraffin sections for morphologic analysis were dewaxed, rehydrated, and stained with hematoxylin and eosin. Paraffin sections were immunostained with Pitx2 antibody (Gift from Tord Hjalt, Lund University, Lund, Sweden) as previously described.[22]

Immunofluorescence Staining on Flat-Mount Retinas and Confocal Imaging

Eyes were enucleated and fixed in 4% paraformaldehyde for 30 minutes, and then marked for future orientation followed by dissection under a regular stereo microscope. Retinas were blocked with blocking buffer A (10% normal goat serum, 0.5% Triton X-100, 0.1M PBS) overnight and then incubated with rabbit anti-RNA-binding protein with multiple splicing (RBPMS) (1830-RBPMS; PhosphoSolutions, Aurora, CA, USA) antibody (1:400) in blocking buffer A at 4° for 3 days. After brief rinse, retinas were incubated with Alexa fluor 488 conjugated goat anti-rabbit IgG (1:200, A-11070; Invitrogen, Waltham, MA USA) in blocking buffer B (5% normal goat serum, 0.5% Triton X-100, 0.1M PBS) at 4° overnight. To stain nuclei, retinas were treated with 0.5 μg/mL DAPI (D-21490; Invitrogen) for 30 minutes. Finally, retinas were mounted onto microscope slides with Fluoromount-G (0100-01; SouthernBiotech, Birmingham, AL, USA). Fluorescence was detected using Leica SP5 confocal microscope (Buffalo Grove, IL, USA). To avoid the potential of introducing bias, the genotypes of all slides were blinded to the operator. Furthermore, the center of the optic nerve head of each retina was identified for the microscope and the software was preprogrammed to acquire images at positions located 1-mm temporal, nasal, superior, and inferior from the optic nerve head (4 images total/retina). RBPMS-positive cells within each blinded image were first counted using Imaris 7.7.1 program (Concord, MA, USA), and then edited by hand. The total number of DAPI[+] nuclei in same images were also quantified in parallel.
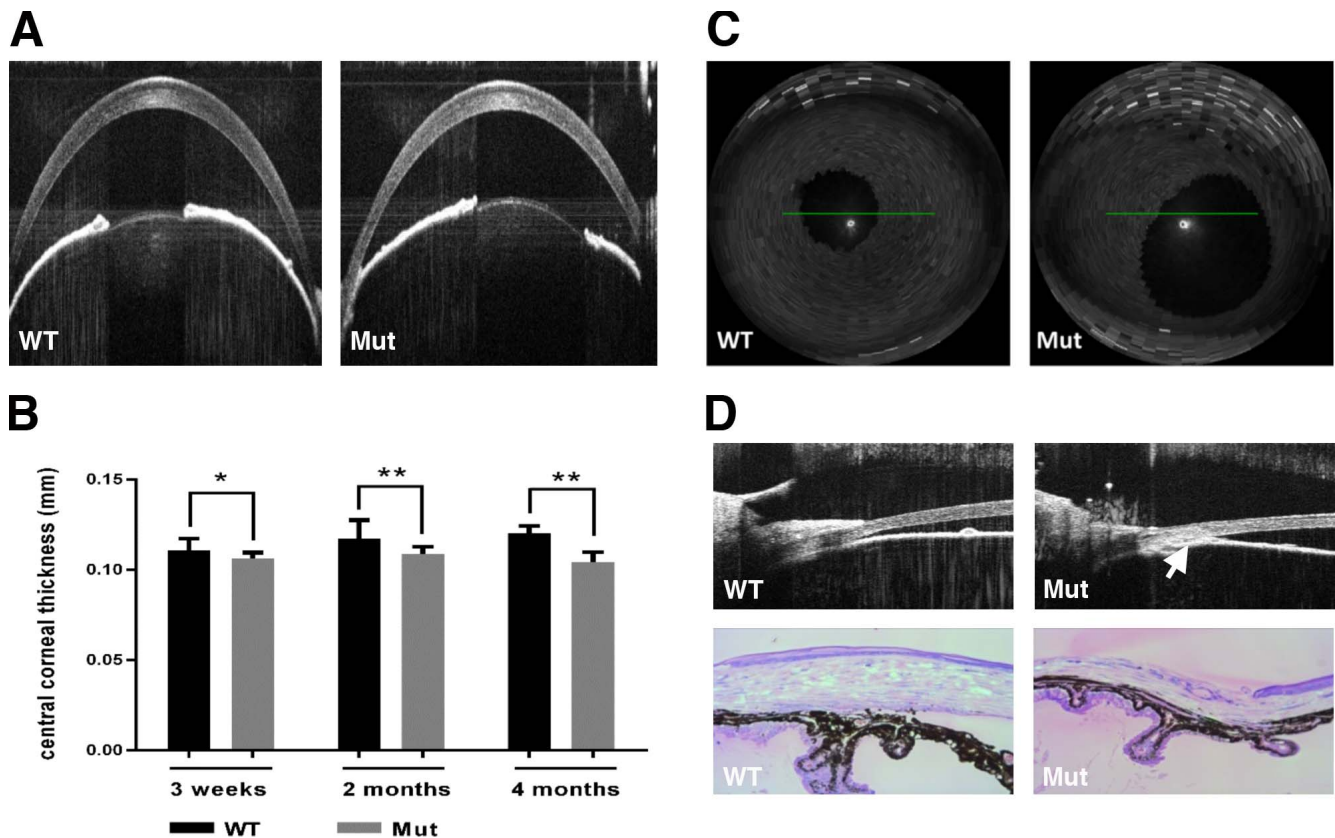
FIGURE 1. Morphologic changes in anterior segments were found in *Pitx2*^{+/−} mice. (**A**) Two representative OCT images showed CCT in wild-type (WT) and *Pitx2*^{+/−} eyes 2 months of age. (**B**) Quantification revealed an increasing reduction in CCT at 3 weeks (4.2%; $N = 18$ WT vs. 14 mutant), 2 months (7.4%; $N = 24$ WT vs. 31 mutant), and 4 months (13%; $N = 23$ WT vs. 26 mutant) in *Pitx2*^{+/−} mice eyes. *Error bars* represent SD. (**C**) Approximately 50% pupils are displaced/enlarged in *Pitx2*^{+/−} mice. (**D**) Anterior synechiae in 2-month-old *Pitx2*^{+/−} eyes was shown either by OCT imaging (*upper panel*, indicated by *red arrow*) or histology. Significance: * $P \leq 0.05$; ** $P \leq 0.01$.

Preparation of Optic Nerve Plastic Sections and *Para*-Phenylenediamine (PPD) Staining

Optic nerves were cut off when eyes were enucleated for flat-mount staining. Specimens were fixed in 3% PFA and 2.5% glutaraldehyde overnight at 4°, and then processed for plastic embedding in Epon by Microscopy & Imaging Analysis laboratory at the University of Michigan. Blocks were cross sectioned at a thickness of 0.5 μm on a Leica Ultramicrotome. To stain optic nerve, sections were immersed in 2% PPD (dissolved in 50% ethanol) for 1 hour, rinsed with distilled water and ethanol, and mounted with Permount (Fisher Biochemicals, Fair Lawn, NJ, USA). Imaging was performed using an Olympus microscope (EX51; Olympus, Center Valley, PA, USA) with ×100 oil objective.

RESULTS

PITX2 Is Expressed Within the Iridocorneal Angle

We showed previously that PITX2 is expressed in ocular neural crest cells at early embryonic stages and subsequently in corneal mesenchyme in developing cornea.[23,24] The features of ARS have been interpreted to mean that PITX2 is also expressed in later-forming structures such as those of the iridocorneal angle, but this has not been experimentally determined. To address this, we immunostained sections from 2-week-old wild-type (WT) mouse eyes and found PITX2 is strongly detected in iridocorneal angle, including the trabecular meshwork and Schlemm's canal (Supplementary Fig. S1).

Weaker expression is also present in the corneal endothelium, corneal stroma, and iris stroma (Supplementary Fig. S1).

Pitx2^{+/−} Mice Have Anterior Segment Dysgenesis Comparable to Axenfeld-Rieger Syndrome

We began analysis of *Pitx2*^{+/−} mice (referred to as "mutant" hereafter) by using spectral-domain optical coherence tomography (SD-OCT) to determine whether their eyes exhibit features of anterior segment dysgenesis that are a hallmark of ARS. We assessed central corneal thickness (CCT) by imaging the corneas in cross-section and found that it is already decreased by 4.2% in mutant eyes ($N = 14$) relative to WT eyes ($N = 18$) at 3 weeks, shortly after eyelid opening (Figs. 1A, 1B). Central corneal thickness is further decreased in the mutant eyes at 2 months (7.4%; $N = 24$ WT vs. 31 mutant) and 4 months (13%; $N = 23$ WT vs. 26 mutant; Fig. 1B), consistent with our previous data analyzing histologic sections.[25] Approximately 50% of mutant eyes have iris defects, including enlarged, displaced, or misshapen pupils, as early as 3 weeks of age (Figs. 1A, 1C). Extensive iridocorneal adhesions (anterior synechiae) resulting in an occluded iridocorneal angle are also apparent by either OCT (Fig. 1D, upper panel) or histology (Fig. 1D, lower panel). Finally, iris hypoplasia and ciliary body atrophy are seen in all mutant eyes (Fig. 1D, lower panel). Collectively, these data suggest that development of multiple anterior segment structures is sensitive to *Pitx2* gene dose, and that heterozygous *Pitx2* mice exhibit multiple anterior segment abnormalities that are consistent with those found in human ARS patients.
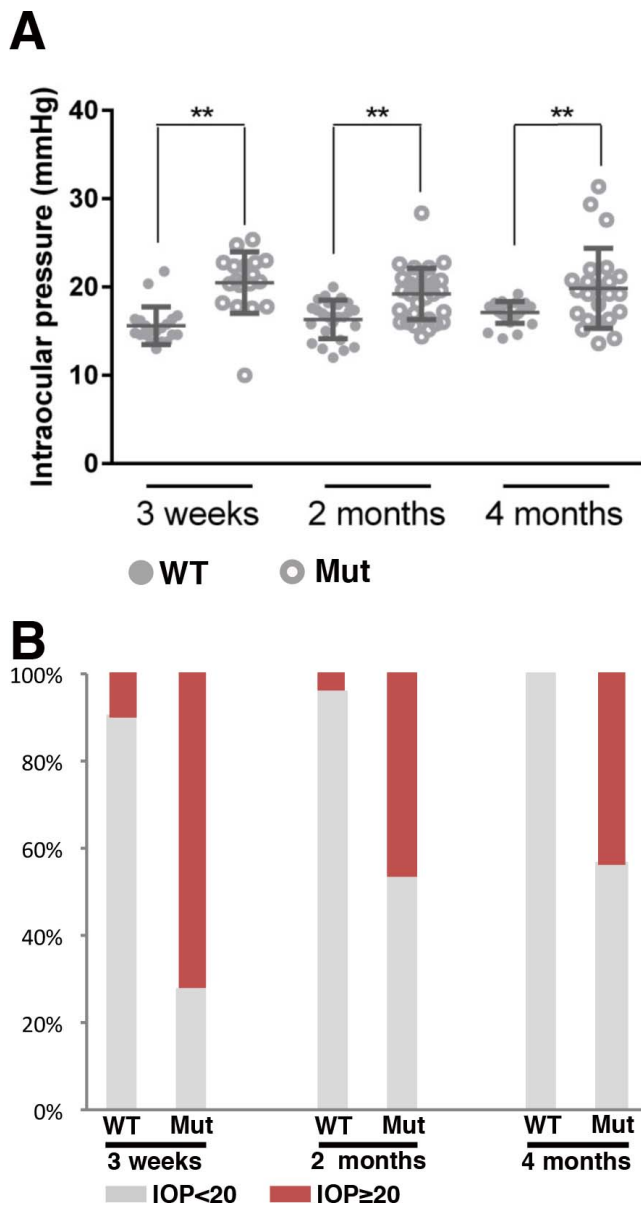
FIGURE 2. Intraocular pressure analysis in the controls and *Pitx2*^{+/−} mice. (**A**) Individual IOP values from the time points indicated were shown by dot plotting. Means ± SD are also included. *Solid circles* represent the values from wild type and *hollow circles* represent the values from *Pitx2*^{+/−}. The mean of IOP values in control eyes was 15.62 ($n = 20$), 15.9 ($n = 25$), and 16.98 ($n = 25$) at 3 weeks, 2, and 4 months, respectively. The mean IOP values for *Pitx2*^{+/−} eyes at 3 weeks, 2, and 4 months of age were 20.5 ($n = 18$), 18.8 ($n = 32$), and 20.1 ($n = 23$), respectively. ** indicates the difference is significant ($P \leq 0.01$). (**B**) Intraocular pressure data are presented by stacked column plotting, showing the percentage of each group at different time points.

Intraocular Pressure Is Elevated in *Pitx2*^{+/−} Mice

The identification of anterior synechiae and occluded iridocorneal angle structures in heterozygous *Pitx2* mice suggested that IOP might be altered in these mice. We initially sought to follow IOP longitudinally on the same cohort of mutants and the control littermates using a TonoLab tonometer. However, this approach rapidly led to opacification and angiogenesis in the corneas of *Pitx2*^{+/−} animals but not WT controls (Chen and Gage, unpublished results). Therefore, to avoid the possibility that changes to the cornea might affect the accuracy of IOP

measurements at the later time points, we used the TonoLab to measure IOP in naïve cohorts of mutant and control mice at each time point (3 weeks, 2, and 4 months of age). In this way, each mouse was only subjected to drug treatment and tonometer measurement only once, and changes to the cornea were not noted.

The mean of IOP values in control eyes was 15.62 ($n = 20$), 15.9 ($n = 25$), and 16.98 ($n = 25$) at 3 weeks, 2, and 4 months, respectively. These values correlate well with previously published standards for the C57BL/6J background on which our *Pitx2*[null] allele is maintained.[26] In contrast, the mean IOP values for *Pitx2*^{+/−} eyes at 3 weeks, 2, and 4 months of age were 20.5 ($n = 18$), 18.8 ($n = 32$), and 20.1 ($n = 23$), respectively ($P < 0.01$ for all groups; Fig. 2A; Supplementary Table S1). Although control eyes rarely have an IOP greater than 20 mm Hg, a significant fraction of *Pitx2*^{+/−} eyes have elevated pressure greater than or equal to 20 mm Hg at all time points examined (Fig. 2B; Supplementary Table S1). Furthermore, reduced CCT in the mutant eyes likely means that we are underestimating their true IOP values. We conclude that a large fraction of *Pitx2*^{+/−} mice are ocular hypertensive, similar to ARS patients.

Optic Nerve Heads Are Defective in *Pitx2*^{+/−} Mice

Deformation of the optic nerve head, frequently referred to as cupping, is a common characteristic of glaucoma. Therefore, we next used SD-OCT to provide in vivo imaging of the posterior eyes of WT and *Pitx2*^{+/−} mice at 3 weeks, 2, and 4 months of age. In control eyes, the optic nerve head uniformly presents as a flat surface at all time points examined (Fig. 3A). In contrast, as early as 3 weeks, moderate to severe optic nerve head cupping is readily apparent in all *Pitx2*^{+/−} eyes examined, and this phenotype persists at subsequent time points examined (Fig. 3A). We also examined optic nerve head appearance using fundus biomicroscopy to confirm these results (Fig. 3B). Taken together, we conclude that *Pitx2*^{+/−} mice have significant optic nerve head cupping that is already fully penetrant by 3 weeks of age.

We have previously reported that optic nerve development is defective in global and neural crest-specific *Pitx2* knockout animals.[21,22] To gain insight into whether optic nerve head development is likely to be affected in *Pitx2*^{+/−} eyes, we examined WT and *Pitx2*^{+/−} eyes at postnatal day 7 using histology, since this time point occurs before the eyelids open and eyes are not accessible to analysis by SD-OCT. For eyes of each genotype, all sections encompassing the optic nerve head were collected and analyzed. We found that optic nerve head histology was indistinguishable between the two genotypes (Fig. 3C). Collectively, these data suggest that the optic nerve head develops normally in *Pitx2*^{+/−} eyes, prior to emergence of a fully penetrant cupping phenotype by 3 weeks of age.

Optic Nerves Are Degenerated in *Pitx2*^{+/−} Mice

Optic nerve degeneration leading to vision loss is a hallmark of glaucoma. To determine axon health, we stained semithin plastic sections taken from optic nerves of *Pitx2*^{+/−} and WT control littermates at 3 weeks and 2 months with *para*-phenylenediamine, which permits sensitive detection of nerve injury by differentially staining single damaged axons.[27] We assigned each nerve into one of four categories based on its health status: (type I) the nerve appeared normal, and no axonal damage was found, (type II) the nerve exhibited regions where axons are dying or absent while other regions contained healthy axons, (type III) no healthy axons can be visibly identified but dying/degenerating axons persist, and (type IV) all axons, including dying ones were gone and gliosis can be
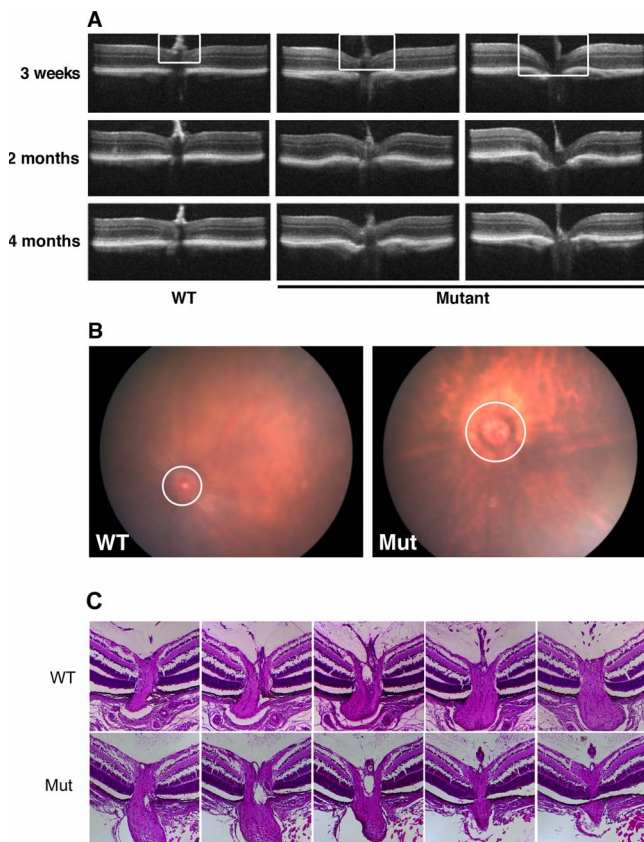
FIGURE 3. Defects of optic nerve head were identified in *Pitx2*^{+/−} mice. (**A**) Eyes from WT and mutant mice were imaged by SD-OCT for morphology of the optic nerve head at the ages indicated. *White rectangle* indicates the region of optic nerve head, where it is flat at all time points in wild type, but cupped with varying severity in the mutants. (**B**) Fundus photography at 2 months also showed morphology of optic nerve head (*circle*) changed in the mutant eyes. (**C**) Representative examples of histologic sections taken through nerve heads from a *Pitx2*^{+/+} and a *Pitx2*^{+/−} eye at postnatal day 7, illustrating the absence of cupping in the heterozygous eyes.

FIGURE 4. Optic nerve degeneration in *Pitx2*^{+/−} mice was identified by PPD staining. (**A**) Representative images of optic nerves from WT and mutant eyes at 2-months old following staining with PPD to visualize the myelin sheath. Optic nerves were assigned to one of four categories based on the severity of degeneration identified: (1) the majority of axons were healthy, (2) partial degeneration was identified regionally, (3) no healthy axons were seen but dying axons were still identifiable, and (4) all axons, including dying ones, were missing. Each type was indicated by a representative image. (**B**) Samples from 3-week-old (WT $N = 12$; mutant $N = 13$) and 2-month-old (WT $N = 8$; mutant $N = 14$) optic nerves were scored based on the severity assignment described previously. At 2 months old, all optic nerves from wild type were healthy and assigned to type I. Degeneration was found in all optic nerves from the mutants with vary severity at 2 months of age, even the density of retinal ganglion cells was normal in the corresponding retinas.

readily identified (Fig. 4A). At 3 weeks of age, 67% (8/12) of wild type have healthy axons as type I, and 33% (4/12) of them were graded to type II. In contrast, mutants of this age exhibit a broader spectrum of phenotypes that could be classified as type I (3/13), type II (4/13), type III (1/13), and type IV (5/13) (Fig. 4B; Supplementary Table S2). At 2 months of age, while all WT optic nerves (8/8) exhibited healthy axons without any detectable signs of degeneration and were classified as type I, no healthy optic nerves that could be classified as type I were identified in the mutants. Rather, the mutant optic nerves also exhibited a spectrum of significant damage that could be classified as type II (6/14), type III (2/14), and type IV (6/14) (Fig. 4B; Supplementary Table S2). Based on these data, we conclude that a majority of optic nerves in *Pitx2*^{+/−} mice already exhibit evidence of glaucomatous degeneration by 3 weeks of age and that all optic nerves in these mice are affected by 2 months of age.

Specific Loss of Retina Ganglion Cells in *Pitx2*^{+/−} Mice

Retina ganglion cell loss is the second hallmark of glaucoma. In addition, our data showing elevated IOP, optic nerve head cupping, complete optic nerve degeneration in the mutant population by 2 months of age suggested the possibility that
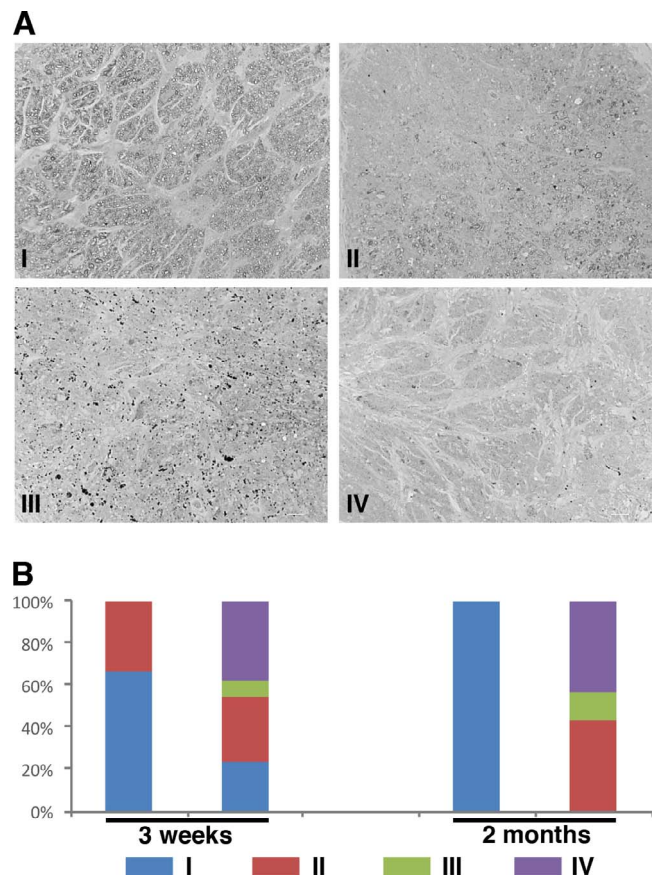
ganglion cells may die in *Pitx2*^{+/−} eyes. Therefore, to visualize RGC content in eyes from control and *Pitx2*^{+/−} mice, whole-mount retinas at 3 weeks and 2 months were immunostained to detect RBPMS, a specific marker for RGCs.[28] To critically assess ganglion cell content in an unbiased manner, we imaged four equivalent prescribed regions each located 1 mm from the optic nerve head (nasal, temporal, superior, and inferior) per retina and quantified ganglion cell density by determining RBPMS^{+} cells per unit area. At 3-weeks old, *Pitx2*^{+/−} images appeared largely normal when compared with control eyes (Fig. 5A). In contrast, a spectrum of reductions in ganglion cell content was readily apparent in images taken from *Pitx2*^{+/−} retinas at 2 and 4 months of age (Fig. 5A and data not shown). Quantitative analysis revealed a small but significant reduction in mean ganglion cell density in the superior quadrant of *Pitx2*^{+/−} eyes at 3 weeks, while other quadrants are unaffected (Fig. 5B). By 2 months of age, although the extent of
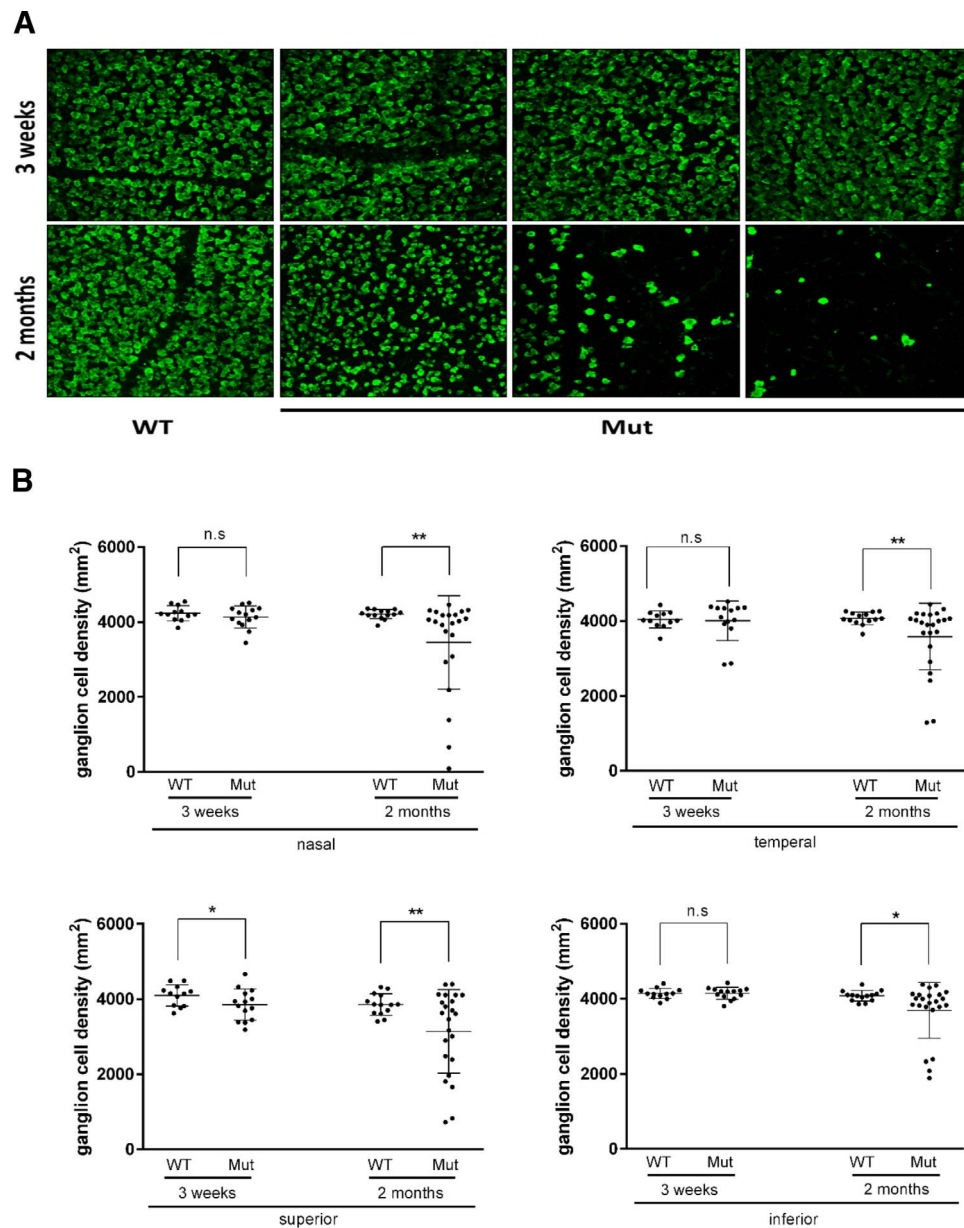
FIGURE 5. Retinal ganglion cell density is reduced in *Pitx2*^{+/−} mice. (**A**) Flat-mounted retinas from 3 weeks, 2, and 4 months were stained with anti-RBPMS antibody, which can recognize specifically RGCs. Representative images from 3-weeks and 2-months old were presented to show fewer retinal ganglion cells in *Pitx2*^{+/−} eyes. At the age of 3 weeks, there was no visible changes in RGC density. However, at the age of 2 months, RGC loss was readily seen with vary severity. (**B**) Retinal ganglion cell density data were analyzed by dot plotting with mean value plus ± SD. Each retina was divided into four areas: nasal, temporal, superior, and inferior. Significance: * $P \leq 0.05$; ** $P \leq 0.01$.

involvement varies greatly between individual eyes, mean RGC density is significantly reduced in all four quadrants of *Pitx2*^{+/−} eyes (Fig. 5B; Supplementary Table S2).

To gain insight into whether additional retinal lineages were likely to be affected in *Pitx2*^{+/−} eyes, we estimated the numbers of displaced amacrine cells, as they represent approximately 50% of the cells present in the ganglion cell layer of WT mouse eyes and would be the most likely lineage to be also affected by generalized effects such as retinal ischemia because they are intimate neighbors of ganglion cells.[29] Because these two lineages together represent the vast majority of cells present in the ganglion cell layer, we deduced the approximate density of displaced amacrine cells in each image used to quantify ganglion cell density by determining the

total number of DAPI[+] nuclei and subtracting the number of RBPMS^{+} cells. We focused on images from 2-month-old heterozygous mice exhibiting a greater than or equal to 35% reduction in ganglion cell number ($N = 13$) in order to maximize our ability to detect any potential changes, as well as 12 randomly chosen images from WT retinas. Based on this analysis, we determined that displaced amacrine cell densities were unaffected in retinae of *Pitx2*^{+/−} eyes, even in samples with severe ganglion cell loss (Fig. 6). Collectively, these data suggest that ganglion cell density is specifically reduced in *Pitx2*^{+/−} eyes by 2 months of age, and that this phenotype emerges later and with reduced penetrance when compared with the degenerative changes to the optic nerve described above.
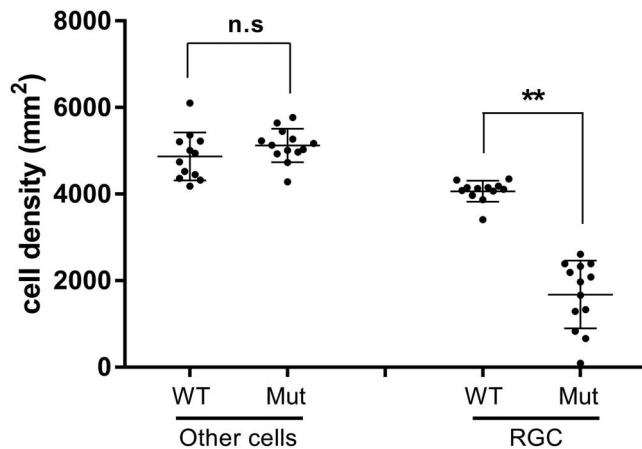
FIGURE 6. Displaced amacrine cell density is unaffected in *PItx2*^{+/−} mice. Comparison of Nonganglion cell densities (other cells) to ganglion cell densities in selected *Pitx2*^{+/+} versus *Pitx2*^{+/−} retinas. Images ($N = 13$) from *Pitx2*^{+/−} retinas exhibiting a $\geq 35\%$ ganglion cell loss of were identified and the density of nonganglion cells "other cells" was deduced by determining the total number of DAPI[+] nuclei and subtracting the number of RBPMS^{+} cells. "Other cells" densities from control images ($N = 12$) were determined in parallel. "Other cells" are presumed to represent displace amacrine cells, as they constitute the vast majority of nonganglion cells in the ganglion cell layer. Data are presented by dot plot with mean values ± SD. Significance: n.s., not significant; ** $P \leq 0.01$.

DISCUSSION

The similarity between human and mouse eyes, coupled with the ability to use a combination of cell biological and genetic tools in mice have led to a large increase in the number of studies using mice as animal models to uncover molecular pathways that control glaucoma pathophysiology. Over the last decades, numerous mice models, including induced experimental models and genetic models, have provided valuable insights into the molecular events that lead to glaucomatous changes.[15,30,31] *Pitx2*^{+/−} mice appear to accurately recapitulate the structural features found in the eyes of ARS patients, as well as the typical hallmarks of glaucomatous eyes, including elevated IOP, reduced RGC density, optic nerve head cupping, and optic nerve degeneration. Notably, these changes emerge either congenitally or at a very early age in these mice, in contrast to previously identified glaucoma models that require significant aging before symptoms begin to emerge. Collectively, these features suggest that these mice provide a powerful new resource for understanding the molecular mechanisms contributing to these phenotypes in ARS patients, and potentially glaucoma more generally. In addition, an early onset, together with complete penetrance of particularly the optic nerve defects, could make use of these mice a very efficient model for developing and testing new neuroprotective therapies.

We found that IOP as measured by rebound tonometry is elevated in a large number of individual *Pitx2*^{+/−} eyes, and that mean IOP within the group is significantly higher than in wild-type siblings. In isolation, the mean values for *Pitx2*^{+/−} eyes at the three time-points measured (20.5, 18.8, and 20.1 mm Hg) could be considered as borderline hypertensive based on standard human criteria.[32] However, CCT is decreased by approximately 10% *Pitx2*^{+/−} eyes and reduced CCT is known to result in underestimation of IOP when IOP is measured by noninvasive methods as was done here.[33] In human patients, there are varying approaches that are used to adjust IOP in order to account for the effects of CCT differences.[33] However, a large meta-analysis of data from human patients indicated a 10%

reduction in CCT resulted in a 3.4 ± 0.9 mm Hg underestimation of IOP when measured by noninvasive methods as compared with direct cannulation.[33] Therefore, although similar analyses have not been performed on mice, it seems reasonable to anticipate that the actual mean pressure in *Pitx2*^{+/−} mutant eyes is even higher than what we have measured here, and that a larger proportion of mutant eyes are expected to have elevated IOP. Even an adjustment of the group mean by 2 to 3 mm Hg argues strongly that the typical *Pitx2*^{+/−} eye is already ocular hypertensive by 3 weeks of age, shortly after eyelid opening.

Our data show that glaucomatous changes to the optic nerve in *Pitx2*^{+/−} eyes occur either congenitally or at a very young age, prior to weaning. The optic nerve heads in *Pitx2*^{+/−} eyes initially appear indistinguishable from WT controls at postnatal day 7; however, obvious cupping is apparent by 3 weeks of age. Degenerative changes in axons of the nerve are also already prevalent by 3 weeks and fully penetrant by 2 months of age. Collectively, the current data are consistent with optic normal development through early postnatal life in *Pitx2*^{+/−} eyes, followed by rapid degeneration. However, we cannot exclude alternative scenarios. Resolution of this issue will require detailed ultrastructural analysis of the optic nerve over the course of its development in both genotypes which, to our knowledge has not yet been done even in WT eyes. It will also be important to address whether these changes only emerge after IOP becomes elevated or whether they arise earlier, suggesting that they emerge independent of pressure. However, we are unaware of any current technologies that would permit reliable assessment of IOP prior to eyelid opening.

Our quantitative sampling of ganglion cell density in eyes of *Pitx2*^{+/−} mice revealed a small but significant reduction in the superior quadrant as early as 3 weeks of age, followed by significant reduction in all four quadrants by 2 months. This suggests that RGCs are lost regionally, instead of uniformly, in *Pitx2*^{+/−} eyes. These changes appear to be specific glaucomatous effects, rather than due to a more general mechanism such as retinal ischemia, as neighboring displaced amacrine cell densities in the ganglion cell layer are unaffected, even in the case of severe ganglion cell loss. These data are also consistent with normal retinal development through early postnatal life, followed by rapid and specific degeneration of the ganglion cells. Strikingly, optic nerve head cupping and degeneration of the nerve itself were consistently more advanced than loss of ganglion cells in *Pitx2*^{+/−} mice at the time points examined, suggesting that these changes might precede RGC death. Interestingly, these observations are consistent with what has been reported in glaucomatous DBA/2J mice.[34,35] Because only a tiny area (located 1 mm away superior, inferior, temporal, and nasal from optic nerve head) was subjected to confocal imaging in our approach in order to reduce the likelihood of experimental bias, it remains unclear whether RGC loss in *Pitx2*^{+/−} mice occurs in the pattern of fan-shaped or pie-shaped sectors of retina extending from the optic nerve head to the periphery and whether this approach may have led to some underestimation of the extent of ganglion cell loss in each retina. Further experiments with whole-mount retina staining will be needed to answer these questions.

Finally, our expression data combined with demonstration of defects in the cornea endothelium and stroma, trabecular meshwork, Schlemm's canal, and iris stroma in *Pitx2*^{+/−} eyes confirm that PITX2 regulates important molecular pathways required for the development and maintenance of these structures that form relatively later during embryogenesis. These roles for PITX2 had been predicted based on the anterior segment dysgenesis that is a hallmark of ARS.[36] Conditional ablation has proved to be powerful tool for understanding the roles of PITX2 in the development of earlier

events during anterior segment development and combining the conditional *Pitx2*^*flox* allele together with appropriate temporally regulated or tissue-specific Cre transgenes will be essential for identifying the essential molecular pathways regulated by PITX2 during development of these late-forming structures. In addition, as more refined tissue-specific Cre transgenes are developed, it is likely that a more refined understanding of the events contributing to glaucoma in ARS will be possible.

References

1. Tham YC, Li X, Wong TY, Quigley HA, Aung T, Cheng CY. Global prevalence of glaucoma and projections of glaucoma burden through 2040: a systematic review and meta-analysis. *Ophthalmology*. 2014;121:2081–2090.

2. King A, Azuara-Blanco A, Tuulonen A. Glaucoma. *BMJ*. 2013; 346:f3518.

3. Mantravadi AV, Vadhar N. Glaucoma. *Prim Care*. 2015;42(3): 437–449.

4. Heijl A, Leske MC, Bengtsson B, Hyman L, Hussein M. Reduction of intraocular pressure and glaucoma progression: results from the Early Manifest Glaucoma Trial. *Arch Ophthalmol*. 2002;120:1268–1279.

5. Quigley HA. Open-angle glaucoma. *N Engl J Med*. 1993;328: 1097–1106.

6. Kwon YH, Fingert JH, Kuehn MH, Alward WL. Primary open-angle glaucoma. *N Engl J Med*. 2009;360:1113–1124.

7. Burgoyne CF. A biomechanical paradigm for axonal insult within the optic nerve head in aging and glaucoma. *Exp Eye Res*. 2011;93:120–132.

8. Nickells RW, Howell GR, Soto I, John SW. Under pressure: cellular and molecular responses during glaucoma, a common neurodegeneration with axonopathy. *Annu Rev Neurosci*. 2012;35:153–179.

9. Paigen K. A miracle enough: the power of mice. *Nat Med*. 1995;1:215–220.

10. Smithies O, Maeda N. Gene targeting approaches to complex genetic diseases: atherosclerosis and essential hypertension. *Proc Natl Acad Sci U S A*. 1995;92:5266–5272.

11. John SW, Smith RS, Savinova OV, et al. Essential iris atrophy, pigment dispersion, and glaucoma in DBA/2J mice. *Invest Ophthalmol Vis Sci*. 1998;39(6):951–962.

12. Anderson MG, Smith RS, Hawes NL, et al. Mutations in genes encoding melanosomal proteins cause pigmentary glaucoma in DBA/2J mice. *Nat Genet*. 2002;30:81–85.

13. Senatorov V, Malyukova I, Fariss R, et al. Expression of mutated mouse myocilin induces open-angle glaucoma in transgenic mice. *J Neurosci*. 2006;26:11903–11914.

14. Zhou Y, Grinchuk O, Tomarev SI. Transgenic mice expressing the Tyr437His mutant of human myocilin protein develop glaucoma. *Invest Ophthalmol Vis Sci*. 2008;49:1932–1939.

15. Fernandes KA, Harder JM, Williams PA, et al. Using genetic mouse models to gain insight into glaucoma: past results and future possibilities. *Exp Eye Res*. 2015;141:42–56.

16. Shields MB, Buckley E, Klintworth GK, Thresher R. Axenfeld-Rieger syndrome. A spectrum of developmental disorders. *Surv Ophthalmol*. 1985;29:387–409.

17. Chang TC, Summers CG, Schimmenti LA, Grajewski AL. Axenfeld-Rieger syndrome: new perspectives. *Br J Ophthalmol*. 2012;96:318–322.

18. Ito YA, Walter MA. Genomics and anterior segment dysgenesis: a review. *Clin Experiment Ophthalmol*. 2014;42:13–24.

19. Reese AB, Ellsworth RM. The anterior chamber cleavage syndrome. *Arch Ophthalmol*. 1966;75:307–318.

20. Fitch N, Kaback M. The Axenfeld syndrome and the Rieger syndrome. *J Med Genet*. 1978;15:30–34.

21. Gage PJ, Suh H, Camper SA. Dosage requirement of Pitx2 for development of multiple organs. *Development*. 1999;126: 4643–4651.

22. Evans AL, Gage PJ. Expression of the homeobox gene Pitx2 in neural crest is required for optic stalk and ocular anterior segment development. *Hum Mol Genet*. 2005;14:3347–3359.

23. Zacharias AL, Gage PJ. Canonical Wnt/beta-catenin signaling is required for maintenance but not activation of Pitx2 expression in neural crest during eye development. *Dev Dyn*. 2010;239:3215–3125.

24. Gage PJ, Kuang C, Zacharias AL. The homeodomain transcription factor PITX2 is required for specifying correct cell fates and establishing angiogenic privilege in the developing cornea. *Dev Dyn*. 2014;243:1391–1400.

25. Asai-Coakwell M, Backhouse C, Casey RJ, Gage PJ, Lehmann OJ. Reduced human and murine corneal thickness in an Axenfeld-Rieger syndrome subtype. *Invest Ophthalmol Vis Sci*. 2006;47:4905–4909.

26. Kim CY, Kuehn MH, Anderson MG, Kwon YH. Intraocular pressure measurement in mice: a comparison between Goldmann and rebound tonometry. *Eye (Lond)*. 2007;21:1202–1209.

27. Sadun AA, Smith LE, Kenyon KR. Paraphenylenediamine: a new method for tracing human visual pathways. *J Neuropathol Exp Neurol*. 1983;42:200–206.

28. Kwong JM, Caprioli J, Piri N. RNA binding protein with multiple splicing: a new marker for retinal ganglion cells. *Invest Ophthalmol Vis Sci*. 2010;51:1052–1058.

29. Schlamp CL, Montgomery AD, Mac Nair CE, Schuart C, Willmer DJ, Nickells RW. Evaluation of the percentage of ganglion cells in the ganglion cell layer of the rodent retina. *Mol Vis*. 2013;19:1387–1396.

30. Bouhenni RA, Dunmire J, Sewell A, Edward DP. Animal models of glaucoma. *J Biomed Biotechnol*. 2012;692609.

31. Iglesias AI, Springelkamp H, Ramdas WD, Klaver CC, Willemsen R, van Duijn CM. Genes, pathways, and animal models in primary open-angle glaucoma. *Eye (Lond)*. 2015;29: 1285–1298.

32. Savinova OV, Sugiyama F, Martin JE, et al. Intraocular pressure in genetically distinct mice: an update and strain survey. *BMC Genet*. 2001;2:12.

33. Doughty MJ, Zaman ML. Human corneal thickness and its impact on intraocular pressure measures: a review and meta-analysis approach. *Surv Ophthalmol*. 2000;44:367–408.

34. Schlamp CL, Li Y, Dietz JA, Janssen KT, Nickells RW. Progressive ganglion cell loss and optic nerve degeneration in DBA/2J mice is variable and asymmetric. *BMC Neurosci*. 2006;7:66.

35. Jakobs TC, Libby RT, Ben Y, John SW, Masland RH. Retinal ganglion cell degeneration is topological but not cell type specific in DBA/2J mice. *J Cell Biol*. 2005;171:313–325.

36. Semina EV, Reiter R, Leysens NJ, et al. Cloning and characterization of a novel bicoid-related homeobox transcription factor gene, RIEG, involved in Rieger syndrome. *Nat Genet*. 1996;14:392–399.